Pergamon

Tetrahedron 56 (2000) 2547–2559

TETRAHEDRON

Reactivity and *endo–exo* Selectivity in Diels–Alder Reaction of *o*-Quinodimethanes. An Experimental and DFT Computational Study

Cristiana Di Valentin, Mauro Freccero,* Mirko Sarzi-Amadè and Riccardo Zanaletti

Dipartimento di Chimica Organica, Università di Pavia, V. le Taramelli 10, 27100 Pavia, Italy

Received 7 December 1999; revised 25 January 2000; accepted 10 February 2000

Abstract—*endo–exo* Selectivity in Diels–Alder cycloadditions of several *o*-quinodimethanes (**1**–**4**) with acrylonitrile, 2-(5H)-furanone and *N*-methylmaleimide has been investigated in acetonitrile solution. Transition structures of the cycloaddition of the parent *o*-QDM (**1**), (*E*,*E*)-1,8-dimethyl-*o*-QDM (**2**), isoindene (**3**) and 2,3-dihydronaphthalene (**4**) with acrylonitrile and maleimide were located at both HF/6-31G* and B3LYP/6-31G* methods. Theoretical data reproduce fairly well both experimental absolute reaction rates and diastereoisomer ratios. The high *endo* selectivity has been rationalized mainly as a result of solvation effects (acetonitrile, PCM model) and reactant deformations. The latter is due to steric interactions. © 2000 Elsevier Science Ltd. All rights reserved.

Introduction

Xylylenes, otherwise known as *o*-quinodimethanes (*o*-QDMs), are a peculiar class of dienes, because they are much more reactive than related 'classical dienes' (such as butadiene and cyclopentadiene) in Diels–Alder cycloaddition reactions (DA) with olefins, and they seem to show higher *endo* selectivity.

o-QDMs have been widely used as intermediates[1] in the synthesis of lignans,[2] terpenes, anthracyclines alkaloids,[3] steroids and other natural products.[4–6] The study of their reactivity, applied to organic synthesis, is still a hot issue, as documented in a very recent review by Martín.[7] Thus, understanding the factors that control the stereochemistry of this DA reaction is of both synthetic and theoretical relevance. Nevertheless, the only computational investigation on *o*-QDMs DA cycloadditions is quite dated.[8]

On the other hand, the literature data on *o*-QDMs *endo–exo* selectivity is far from being clearly rationalized. The *endo–exo* ratio has been reported to be dependent both on the nature of the dienophiles and on the substituents at the *o*-QDM α-positions. α-Hydroxy, α-alkoxy and α-acetoxy-*o*-QDMs cycloadd to dienophiles such as maleic anhydride and dimethyl maleate by *endo* addition.[9] The presence of a phenyl group[9] at the α position of the *o*-QDM reverses the stereochemical outcome of the reaction. In fact α-phenyl-*o*-QDM and (*E*,*E*)-α-alkoxy-α′-phenyl-*o*-QDM react with dimethylmaleate and crotonate by *exo* orientation, showing a 90% *exo* diastereoselectivity.[9,10] The mild conditions used ($T < 80°C$) 'exclude the possibility of a reversible DA reaction and one is left with the conclusion that at least in some cases *exo* approach to aryl substituted *o*-QDMs does occur'.[1] α-Alkyl-*o*-QDMs seem to react with dienophiles with a lower degree of *endo* selectivity, but this statement is based on a very limited number of substrates.[10]

Secondary orbital interactions (in particular with highly reactive electron poor dienophiles such as maleic anhydride),[11] steric repulsion[12] and even hydrogen bonding[1] (for α-hydroxy-*o*-QDMs) have been suggested as controlling factors of the diastereofacial selectivity in these cycloaddition reactions.

More recently Wagner and coworkers pointed out the importance of the structure of photogenerated *o*-xylylenols (*E*, *Z* isomers), arising from a twisted triplet *o*-xylylenol intermediate, in the control of the stereoselectivity of their Diels–Alder reactions.[13] The author demonstrated that the diastereoisomer adduct ratio of α-hydroxy-α′-phenyl-*o*-QDM addition to maleic anhydride (*endo*:*exo*=4:1)[14] actually is the result of competing *endo* Diels–Alder reaction on two isomeric *o*-xylylenols and not the outcome of competing *endo–exo* additions on the same geometrical isomer.

The latter work emphasizes the obvious observation that the same stereochemical outcome in α,α′-disubstituted-*o*-QDM

Keywords: *o*-quinodimethanes; Diels–Alder reactions; diastereoselection; transition states.

* Corresponding author. Tel.: +39-382-507668; fax: +39-382-507323; e-mail: freccero@chifis.unipv.it

PII: S0040-4020(00)00126-5

DA reaction can be rationalized either in terms of *endo* (or *exo*) competing cycloadditions on two geometrical isomers or in terms of a competition between *endo* and *exo* cycloaddition on only one geometrical isomer. Thus, an investigation focused on the controlling factors of the DA diastereoselectivity for α,α′-disubstituted-*o*-QDMs has to choose carefully the derivatives whose DA reactions involve just one geometrical isomer and not an isomer mixture (i.e. *EE*, *EZ*, *ZE* and *ZZ*).

o-Quinodimethanes with α-alkyl substituents represent appealing substrates to study the diastereoselectivity problem in DA reactions for at least two reasons: (i) they allow one to evaluate experimentally (through the adducts stereochemistry) the *endo*–*exo* approach of the dienophiles, while at the same time, (ii) alkyl substituents should not appreciably modify the *endo*–*exo* orienting electronic effects typical of the *o*-QDM moiety. Thus, the study of such substrates should allow an evaluation of the role of the *o*-QDM moiety in the control of *endo*–*exo* selectivity.

For the above reasons, we considered worthwhile an experimental and computational investigation centered on the comparison of reactivity of three α,α′-dialkylsubstituted *o*-QDMs [namely, (*E*,*E*)-1,8-dimethyl-*o*-QDM (**2**), isoindene (**3**) and 2,3-dihydronaphthalene (**4**)] with electron poor dienophiles [i.e. acrylonitrile, 2-(5H)-furanone and *N*-methylmaleimide (maleimide in the computational study)] with that of the parent *o*-QDM **1** with the same dienophiles.

The aim of our investigation was firstly to assess unambiguously the stereochemical outcome by using *o*-QDMs having a well known configuration and then to reproduce at the B3LYP/6-31G* level of theory the absolute reaction rates as well as the *endo*–*exo* selectivity of the above *o*-QDMs, in order to quantitatively evaluate the controlling effects of the diastereoselectivity of such DA cycloadditions.

To the best of our knowledge this is the first attempt to rationalize the *endo*–*exo* selectivity of *o*-QDM Diels–Alder cycloadditions with a computational investigation at DFT level of theory.

Experimental

Generation of *o*-QDMs and their trapping with dienophiles

o-QDM (**1**), (*E*,*E*)-1,8-dimethyl-*o*-QDM (**2**), isoindene (**3**) and 2,3-dihydronaphthalene (**4**) (see Scheme 1) have been generated in situ by a 1,4 elimination triggered by fluoride anion (with solid potassium fluoride, at 80°C, for the less reactive dienophiles, or an acetonitrile solution, at room temperature of tetrabutyl ammonium fluoride) added to an acetonitrile solution of the corresponding [α-[*o*-[α-(trimethylsilyl)alkyl]phenyl]alkyl]trimethyl ammonium iodide, according to the method of Ito, Nakatsuka and Saegusa.[10]

As already reported, *o*-quinodimethanes generated in situ dimerize in absence of reactive dienophiles to produce spiro dimers. The generation of *o*-QDMs in the presence of various dienophiles provided cycloadducts in fairly good yields.[10]

Cycloadditions of *o*-QDM 1

o-QDM **1** generated in situ from [*o*-((trimethylsilyl)-methyl)benzyl] trimethylammonium iodide (**5**) can be trapped efficiently by acrylonitrile, 2-(5H)-furanone and *N*-methyl maleimide to give DA cycloadducts **9**, **10** and **11**, respectively (Scheme 2).

Cycloadditions of (*E*,*E*)-1,8-dimethyl-*o*-QDM (2)

α,α′-Dimethyl-*o*-QDM (**2**) generated in situ from a 3:2 diastereoisomeric mixture of [α-[*o*-[α-(trimethylsilyl)ethyl]-phenyl]ethyl]trimethylammonium iodide (**6**)[10] (Scheme 1) reacted with *N*-methyl maleimide to give a single cycloadduct (**13endo**) (Scheme 2).

The *endo* stereochemistry and the *cis* relationship between the two methyl groups of **13endo** have been unambiguously established by X-ray analysis.[15] Since it looks highly unlikely that this product comes from a complete *exo* diastereoselective cycloaddition on the much less stable diastereomeric (*Z*,*Z*)-α,α′-dimethyl-*o*-QDM [notice (see below) that (*Z*,*Z*)-cyclic,disubstituted-*o*-QDM, i.e. **3** and **4**, afforded only *endo* adducts with *N*-methylmaleimide], we can safely assume that it derives from the *endo* cycloaddition on (*E*,*E*)-α,α′-dimethyl-*o*-quinodimethane (**2**).

The complete (*E*,*E*) diastereoselectivity in the formation of **2**, i.e. the absence of (*E*,*Z*) isomers even starting from a mixture of diastereoisomeric iodides **6**, is noteworthy. This peculiarity was already underlined by Ito, Nakatsuka and Saegusa[10] in the cycloaddition of **2** with dimethyl fumarate.

The cycloaddition reaction of **2** with acrylonitrile affords a **12endo**–**12exo** (86:14) mixture (Scheme 2). The stereochemistry of cycloadducts **12endo** and **12exo** has been

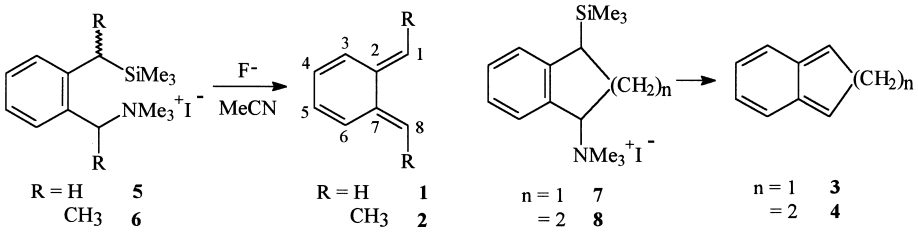

Scheme 1.

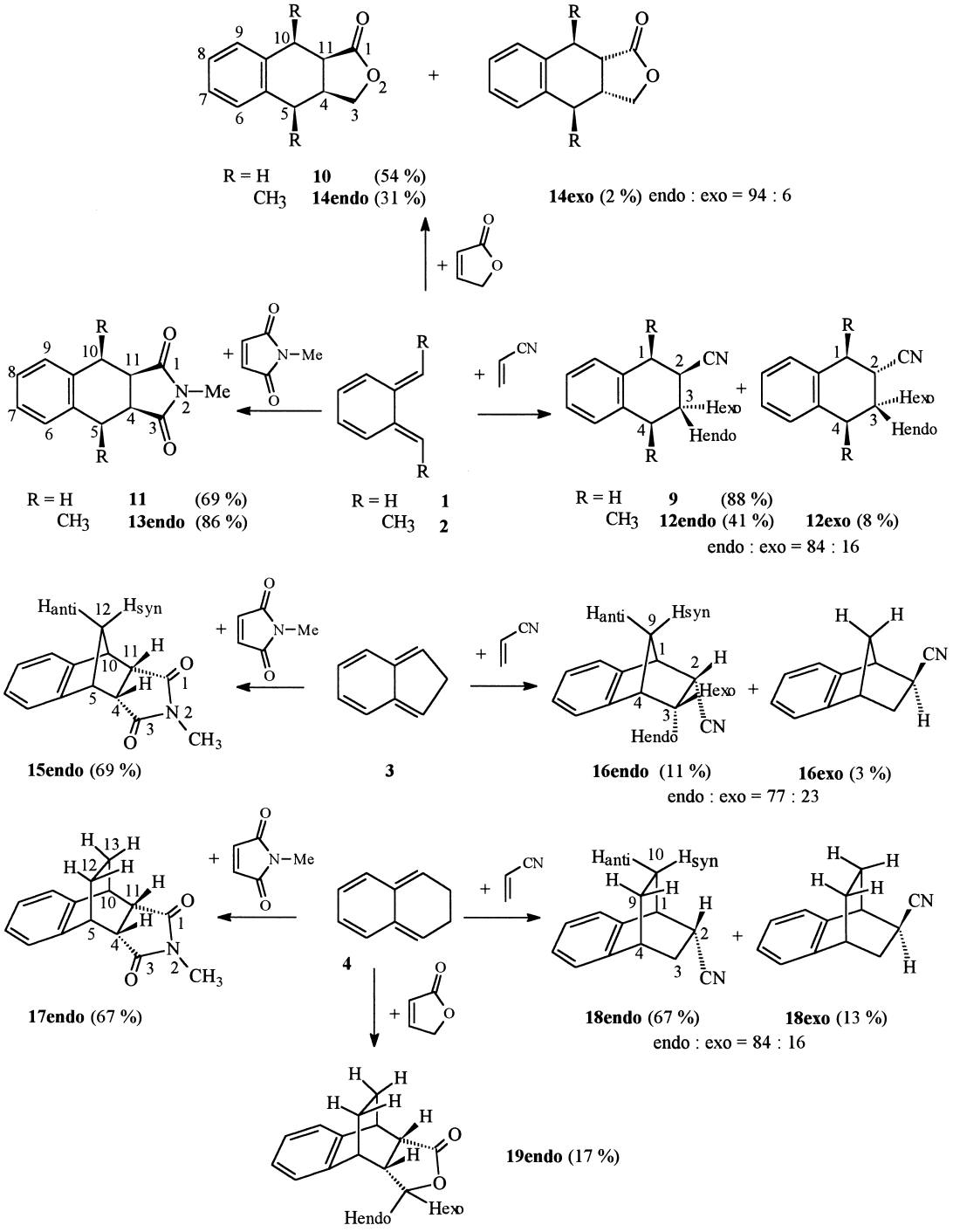

Scheme 2.

assigned on the basis of the ^{1}H NMR coupling constants and NOE effects.

The ring proton H-2 in **12endo** (3.02–3.10 ppm), α to the cyano group (Fig. 1), appears as a ddd ($J_{2,3ax}$=12.2 Hz, $J_{1,2}$=4.9 Hz, $J_{2,3eq}$=3.4 Hz) whose largest *J* (with H-3ax) is certainly the result of an axial–axial coupling while the other two *J*s indicate axial–equatorial relationships. These observations establish H-2 as axial, the CN group as equatorial and the neighboring benzyl methyl group at C-1 as axial. The equatorial position of the C-4 methyl group, and consequently its *cis* relationship to the C-1 methyl group, is supported by couplings involving the benzyl proton H-4. In fact, this proton occurs as a multiplet with an axial–axial coupling to H-3ax, that is, $J_{3ax,4}$= 11.1 Hz. The relative configuration of the C-1 and C-4 stereogenic centers in **12endo** was confirmed by NOE experiments: irradiation of the proton at δ 1.85 (H-3ax) gave rise to NOE effect for the signals of both the methyl groups, Me-1 (2.5%) and Me-4 (2.0%), as indicated in Fig. 1.

In the *exo* isomer (**12exo**) the H-2 proton (2.78 ppm)

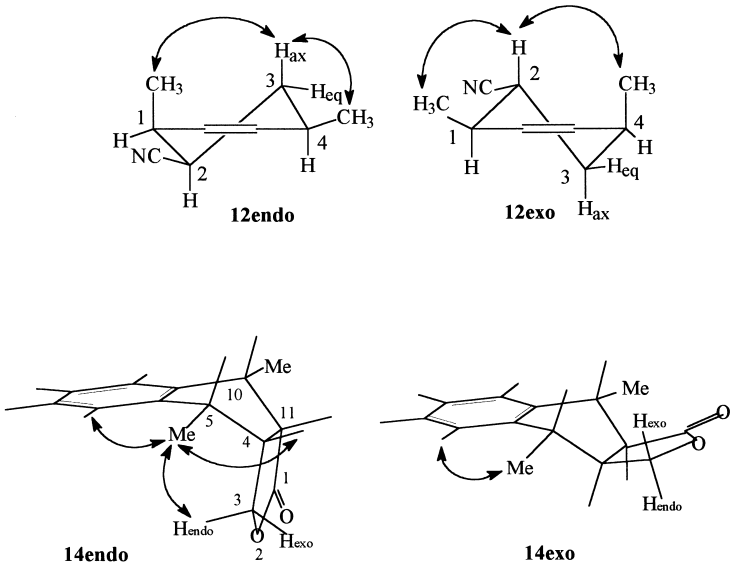

Figure 1. Selected NOE enhancements on **12** and **14** *endo–exo* isomers.

appears as a ddd showing a small $J_{2,3eq}$=3.8 Hz and two relatively large coupling constants ($J_{1,2}$=8.0 Hz and $J_{2,3ax}$=9.0 Hz). This evidence suggests that H-2 is involved in an axial–equatorial as well as two axial–axial couplings. Therefore, H-2 is axial while the geminal CN group and the Me group at C-1 are equatorial and, thus, *trans* to each other.

The relative configuration of the C-4 stereogenic center (in particular the axial orientation of Me-4) in adduct **12exo** was established by observation that irradiation of the proton at δ 2.78 (H-2) gave rise to NOE effects for the signals of both Me-1 (1.9%) and Me-4 (2.7%) as indicated in Fig. 1. Thus, Me-1, H-2 and Me-4 are *cis* to each other.

The cycloaddition of **2** with 2-(5H)-furanone afforded a mixture of adducts, **14endo**–**14exo**=94:6 (Scheme 2), whose structure, in particular *endo–exo* stereochemistry, has been assigned on the basis of ^{1}H NMR data associated with the result of decoupling and NOE experiments. The ^{1}H NMR spectrum of the more abundant of these adducts, i.e. **14endo**, exhibited two doublets at δ 0.82 and 1.68, respectively, which are attributable to Me-5 and Me-10 (see Scheme 2). Irradiation of the higher field doublet made the multiplet centered at δ 2.20 collapse to a doublet ($J_{4,5}$=5.0 Hz) while irradiation of the lower field doublet led to high simplification of the multiplet centered at δ 2.38. These observations demonstrate that these two multiplets can be attributed to H-5 and H-10, respectively. Proton H-3*endo* (δ 3.05, dd) and H-3*exo* (δ 3.45, dd) are coupled to each other ($J_{3endo,exo}$=9.3 Hz) and both, as shown by decoupling experiments, to H-4 (multiplet at δ 2.28, $J_{3endo,4}$=6.3 and $J_{3exo,4}$=9.3 Hz).

The *endo* stereochemistry of this adduct rests firmly on NOE experiments (see Fig. 1). In fact, saturation of Me-5 (at δ 0.82) gave rise to increase in signal intensity of H-3*endo* (1.6%), of the aromatic proton H-6 (2.8%), and of H-4 (2.0%) while saturation of H-3*endo* (δ 3.05) brought about a significant NOE effect in the Me-5 signal (2.7%).

Consistently, irradiation of Me-5 (at δ 0.80) in **14exo** induced a signal enhancement for the close aromatic proton H-6 (2.5%), but did not lead to any measurable NOE for the H-3*endo* signal.

Cycloadditions of isoindene (3)

Isoindene (**3**) generated in situ from (1-(trimethylsilyl)-indan-3-yl)trimethyl ammonium iodide (**7**) (Scheme 1), adds to N-methyl maleimide to give a single *endo* (**15endo**) cycloadduct (Scheme 2). Similarly, N–H maleimide gave a single *endo* cycloadduct. Saturation of H-12*syn* (Scheme 2) increased the signal intensity of both H-4 and H-11 by 3.5% thus proving the *endo* stereochemistry of this cycloadduct.

3 adds to acrylonitrile to afford a **16endo**–**16exo** (77:23) mixture in poor yields (14%). Indene is the main product (80% yield) of the reaction. The product distribution analysis suggests that the DA cycloaddition reaction does not compete efficiently with [1,5]-H shift. No dimers were detected in the crude reaction. This is the case, as well, for the cycloaddition of **3** with 2-(5H)-furanone, where no DA cycloadducts were detected in the reaction mixture. Long range couplings allowed an easy choice between the *endo* and *exo* structure in the case of adducts **16**. H-9*anti* in **16endo** is coupled with H-3*endo* through a long range *W* coupling constant ($J_{3endo,9anti}$=2.7 Hz) whereas it does not show any measurable coupling constant with H-2 (which occupies an *exo* position). On the other hand, in **16exo**, a *W* coupling path connects H-2 (now in *endo* position) and H-9*anti* and consistently the related long range coupling constant ($J_{2,9anti}$=2.5 Hz) is observed.

Cycloadditions of 2,3-dihydronaphthalene (4)

2,3-Dihydronaphthalene (**4**) generated in situ from a 7:3 diastereoisomeric mixture of (1-(trimethylsilyl)-1,2,3,4-tetrahydronaph-4-yl)trimethylammonium iodide (**8**) (Scheme 1), reacted with *N*-methyl maleimide. A single cycloadduct,

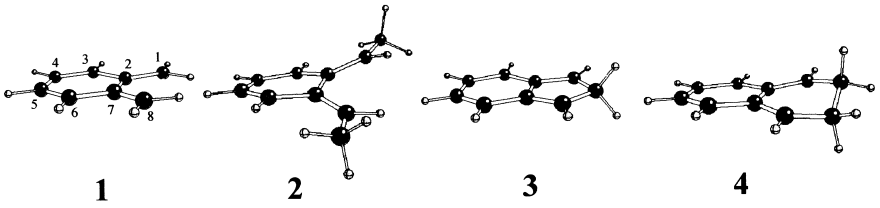

Figure 2. *o*-QDMs **1**–**4** optimized geometries at B3LYP/6-31G* level.

i.e. **17endo**, was obtained in fairly good yield (67%). Analogously to N–Me maleimide, maleimide cycloadds to **4** with a complete *endo* selectivity. NOE experiments and X-ray analysis[15] did not leave any doubt about its *endo* stereochemistry. Irradiation of H-4 and H-11 (Scheme 2) brought about an increase in the H-12*syn* and H-13*syn* signal intensity by 3.0%.

The cycloaddition with acrylonitrile affords an adduct mixture, **18endo**–**18exo**=84:16, in good yields (80%), in agreement with the results already published by Ito (8:1).[10] The stereochemistry of the *endo* cycloadduct has been assigned on the basis of the finding that irradiation of H-2 brought about an NOE enhancement of H-9*syn* and H10-*syn* by 3.3%. No NOE effects were detected on H-9*syn* and H-10*syn* on irradiation of H-2 in **18exo**.

Cycloaddition of **4** with 2-(5H)-furanone gave pure **19endo**. No *exo* isomer was detected in the crude reaction mixture by ^{1}H NMR analysis. Irradiation of H-3*endo* led to enhancement of the H-5 signal by 2.3% in accord with the *endo* stereochemistry of this adduct.

Computational Methods

The energies and geometries of the reactants (Fig. 2), adducts as well as of the transition structures (TSs) (Figs.

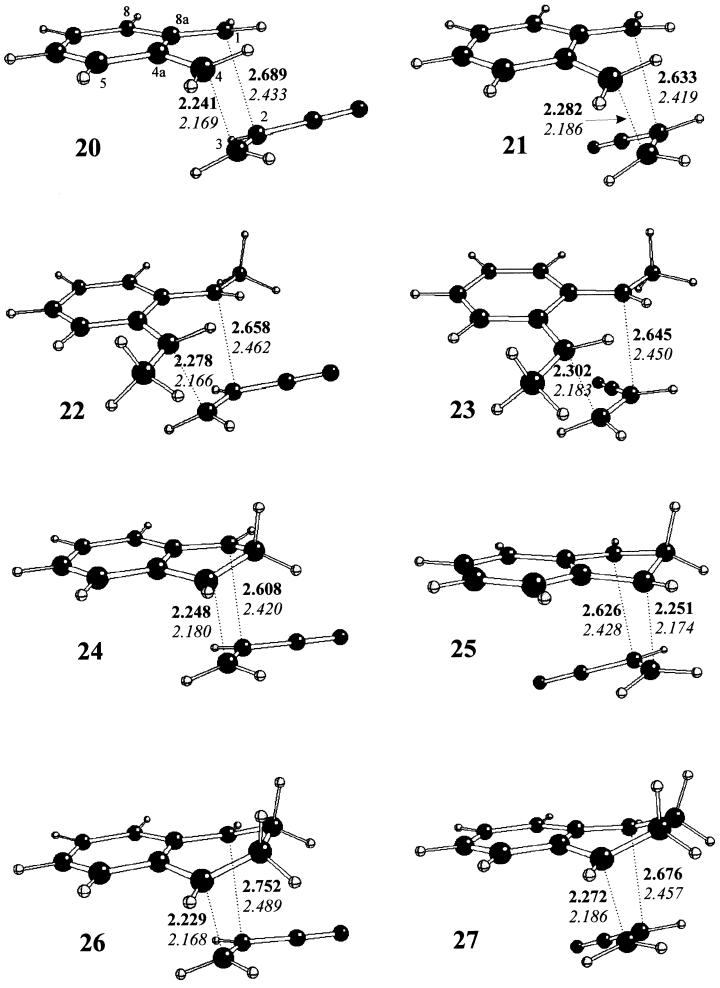

Figure 3. *Exo* and *endo* transition structures (TSs) for the DA cycloadditions of acrylonitrile with *o*-QDMs **1**, **2**, **3** and **4**, respectively, optimized at B3LYP/6-31G* level. Forming bond lengths in the optimized TSs at B3LYP/6-31G* and HF/6-31G* levels are given in bold and italic characters, respectively. All bond lengths are in angstroms (Å).

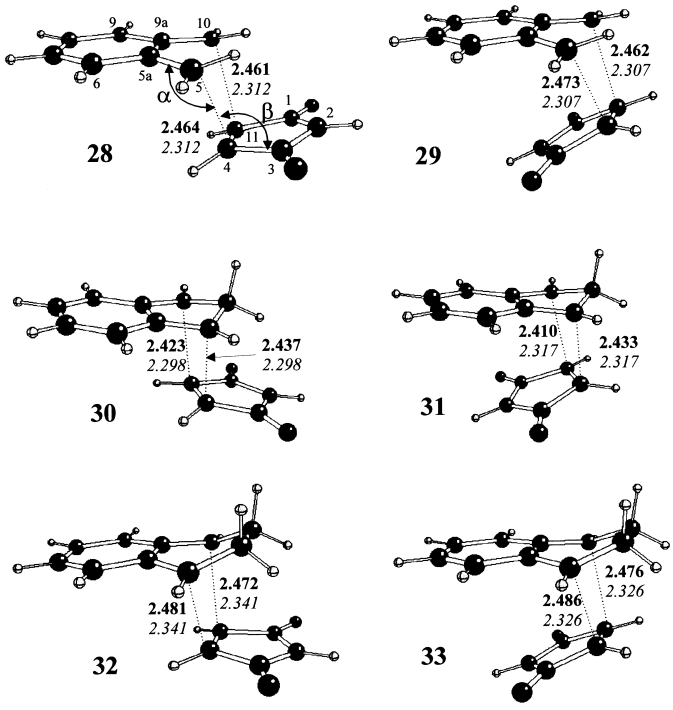

Figure 4. *Exo* and *endo* transition structures (TSs) for the DA cycloadditions of maleimide with *o*-QDMs **1**, **3** and **4**, respectively, optimized at B3LYP/6-31G* level. Forming bond lengths in the optimized TSs at B3LYP/6-31G* and HF/6-31G* levels are given in bold and italic characters, respectively. All bond lengths are in angstroms (Å).

3 and 4) were calculated with both HF/6-31G* method and with density functional theory (DFT) using the Becke3-LYP functional[16,17] and the 6-31G* basis set. All calculations were performed with the GAUSSIAN 94 suite of programs.[18] Critical points have been characterized by diagonalizing the Hessian matrices calculated for the optimized structures; transition structures have only one negative eigenvalue (first-order saddle points) with the corresponding eigenvector involving the expected formation of the two new carbon bonds C_1C_2 and C_3C_4.

In order to produce theoretical activation parameters, vibrational frequencies (in the harmonic approximation) were calculated for all the optimized B3LYP/6-31G* structures and used, unscaled, to compute the zero point energies, their thermal corrections, the vibrational entropies, and their contributions to activation enthalpies, entropies and free enthalpies. The computed electronic energies for the reactants and transition structures (TSs) and the thermodynamic activation parameters, obtained from gas phase vibrational frequencies, are listed in Table 2.

Table 1. Forming bond length and dihedral angles (α and β) in TSs (B3LYP/6-31G*) with maleimide

TS		C_4C_5[a]	$C_{10}C_{11}$[a]	α[b]	β[b]
28	**exo**	2.464	2.461	112.77	99.86
30		2.437	2.423	99.08	102.97
32		2.481	2.472	103.95	106.67
29	**endo**	2.473	2.462	116.39	102.39
31		2.433	2.410	103.46	102.23
33		2.486	2.476	110.04	103.82

[a] Bond length in Å.
[b] Angles in degree (see text and Fig. 4 for the definition of α and β angles).

The contribution of solvent effects to the activation free enthalpy of the reactions under study are calculated via the self-consistent reaction field (SCRF) using the Tomasi model (interlocking spheres) by single point calculations (i.e. with unrelaxed gas-phase geometries of reactants and TSs) at the B3LYP/6-31G* level.[19] Table 2 contains the solvent effect on activation Gibbs free energy, computed according to Tomasi PCM model for acetonitrile as solvent (ϵ=35.9).

Computational Results and Discussion

Experimental data show the *endo* attack on **2**, **3** and **4** as highly predominant even for a dienophile such as acrylonitrile (86, 77 and 84% *endo* adducts, respectively), which has always shown a negligible *endo* selectivity with classical dienes.[20] Somewhat surprisingly diastereoselectivity does not significantly change on changing the *o*-QDM derivative, in particular on passing from QDM **2** [with acyclic (*E*,*E*)-dimethyl substitution] to QDM **3** [with cyclic (*Z*,*Z*)-dimethylene substitution].

Complete *endo* selectivity is observed experimentally with a more reactive dienophile such as N–Me maleimide for all *o*-QDMs **2**–**4**.

In order to clarify the controlling factors of such a high *endo* selectivity we carried out ab initio calculation at both HF/6-31G* and B3LYP/6-31G* level of theory, for the cycloaddition reactions of **1**–**4** with acrylonitrile and maleimide,

Table 2. Calculated activation parameters in gas-phase (at 298 K) for *o*-QDM **1**–**4** Diels–Alder reactions, with acrylonitrile (**20**–**27**) and maleimide (**28**–**33**) at the B3LYP/6-31G* (HF/6-31G*) level[d]

Structures	E (Hartree)	$\Delta E^{\neq}$	$\Delta\Delta E^{\neq}$[a,c]	$\Delta H^{\neq}$	$\Delta S^{\neq}$	$\Delta G^{\neq}$	$\Delta\Delta G^{\neq}$[b,c]
exo TS **20**	−480.4283011	5.77 (26.72)	0.83 (0.74)	7.88	−28.90	16.50	0.89 (0.76)
endo TS **21**	−480.4269891	6.60 (27.47)		8.63	−29.36	17.39	–
exo TS **22**	−559.0623486	5.40 (26.68)	0.74 (0.62)	6.92	−35.64	17.54	0.72 (0.64)
endo TS **23**	−559.0611666	6.14 (27.29)		7.55	−35.93	18.26	
exo TS **24**	−518.5475298	6.80 (25.13)	0.59 (0.51)	8.46	−33.44	18.42	0.64 (0.50)
endo TS **25**	−518.5465850	7.39 (25.64)		9.01	−33.71	19.06	
exo TS **26**	−557.8559783	11.21 (32.58)	0.94 (0.34)	12.82	−32.35	22.46	0.80 (0.14)
endo TS **27**	−557.8544747	12.15 (32.92)		13.63	−32.32	23.26	–
exo TS **28**	−669.0287195	3.86 (23.77)	−1.30 (−1.82)	5.89	−29.61	14.72	−0.92 (−1.45)
endo TS **29**	−669.0307918	2.56 (21.95)		4.57	−30.98	13.80	–
exo TS **30**	−707.1480376	4.83 (23.01)	−0.93 (−2.14)	6.46	−34.35	16.70	−0.59 (−1.73)
endo TS **31**	−707.1495153	3.90 (20.87)		5.55	−35.47	16.11	
exo TS **32**	−746.4549065	10.23 (31.16)	−2.44 (−3.81)	11.79	−33.80	21.87	−2.26 (−3.67)
endo TS **33**	−746.4587941	7.79 (27.35)		9.28	−34.65	19.61	–

[a] $\Delta\Delta E^{\neq}=\Delta E^{\neq}_{endo}-\Delta E^{\neq}_{exo}$: *endo*–*exo* relative electronic activation energy.
[b] $\Delta\Delta G^{\neq}=\Delta G^{\neq}_{endo}-\Delta G^{\neq}_{exo}$: *endo*–*exo* relative Gibbs free activation energy.
[c] A negative value means a more stable *endo* TS, vice versa a positive value means a more stable *exo* TS. Electronic energies (in Hartree) of the reactants: acrylonitrile: E=−170.8315508, N–H maleimide: E=−359.4289178, **1**: E=−309.6059506, **2**: E=−388.2394072, **3**: E=−347.7268126, **4**: E=−387.042294.
[d] Energies in kcal mol^{-1}, entropy in eu; standard state (298 K) of the molar concentration scale (gas in ideal mixture at 1 mol l^{-1}, P=1 atm); $\Delta E^{\neq}$ is the electronic activation energy; $\Delta H^{\neq}$, $\Delta G^{\neq}$ are the molar enthalpy and free Gibbs energy, $\Delta S^{\neq}$ is the molar activation entropy. For conversion from 1 atm standard state to 1 mol l^{-1} standard state (both for gas-phase) the following contributions need to be added to standard enthalpy, free Gibbs energy, and entropy, respectively: $-RT$, $RT\ln R'T$, $-R\ln R'T-R$, where R′ is the value of the R constant given in l atm mol^{-1}K^{-1}. For a reaction with A+B=C stoichiometry, the corrections for $\Delta H^{\neq}$, $\Delta G^{\neq}$ and $\Delta S^{\neq}$ are RT, $-RT\ln R'T$, $R\ln R'T+R$. At 298 K the corrections amount to 0.59 and −1.90 kcal mol^{-1} for $\Delta H^{\neq}$ and $\Delta G^{\neq}$, respectively, and 8.34 eu for $\Delta S^{\neq}$. A further correction of $R\ln 4$ to $\Delta S^{\neq}$ (and consequently $RT\ln 4$ to $\Delta G^{\neq}$) has to be added to take into account statistic effects.

which show respectively, the lowest and the highest *endo* selectivity.

We were able to locate both the *endo* and *exo* TSs for the cycloadditions of **1**–**4** with acrylonitrile (Fig. 3) as well as for the reactions of **1**, **3** and **4** with parent maleimide (Fig. 4). Our aim was to produce not only geometries but also reliable relative (*endo*–*exo*) and absolute energies, in order to properly describe the competing *endo*–*exo* pathways taking into account the solvent effect as well.

First, for sake of clarity, we will discuss the transition structures and *endo*–*exo* selectivity for the reactions of QDMs with each dienophile, one at a time. Then, the absolute rate constants and the *endo*–*exo* selectivity are addressed in comparison with experimental data.

o-QDMs structures

Full geometry optimization was carried out for the *o*-QDMs **1**–**4**. Both *o*-QDMs **1** and **3** have planar structures (Fig. 2).

The deviation from planarity of the diene moiety, evaluated from the dihedral angle $C_1C_2C_7C_8$ (Fig. 2 for numbering), is moderate in **4** (12°) and much more pronounced in **2** (28.0°). It is accompanied by a slight conrotatory rotation around the C_1C_2 and C_7C_8 bonds. The optimized geometries show a clearcut single–double bond alternation (for instance C_1C_2=1.353, C_2C_3=1.462, C_3C_4=1.351 Å in **1** and C_1C_2=1.362, C_2C_3=1.443, C_3C_4=1.360 Å in **3**), which decreases in the order **1**>**2**>**4**>**3**. The stability of SCF solution for the optimized structures **1**–**4** (at the B3LYP/6-31G* level) has been successfully tested. Such stability, at this level of theory, indicates that the lowest energy wavefunction for all *o*-QDMs studied is a closed shell singlet and not a diradical, even for *o*-QDMs **2** and **4** which show significant deviation from planarity. UB3LYP/6-31G* calculation reveals that the *o*-QDM triplet shows a planar structure with an aromatic ring. In fact the diradical species does not show any single–double bond alternation of the inner bonds (C_2C_3=1.405, C_3C_4=1.407 Å). The spin density (0.85) is mainly located on the *exo* CH_2 groups of such a diradical species. The electronic energy is 22.28 kcal mol^{-1} higher than that of the closed shell *o*-QDM **1**.

Transition structures of *o*-QDMs 1–4 with acrylonitrile

Looking at the TS geometries, the most significant parameters that change with the introduction of the electronic correlation (at DFT level) are the forming bond distances. A comparison between HF/6-31G* and DFT calculations reveals that DFT TSs (Fig. 3) always exhibit longer incipient bond lengths than the corresponding HF TSs and that this difference is more pronounced for the longer C_1--C_2 bond than for the shorter C_3--C_4 bond (see Fig. 3 for numbering). As a result, forming bond length asynchronicity predicted by HF calculations for TSs of cycloadditions between **1**–**4** and acrylonitrile is enhanced on passing to DFT calculations. At the latter theory level the forming bond length asynchronicity spans the range from 0.52 Å, for *exo* TS **26** to ≈0.35 Å for TSs **21**, **24** and **25**.

The forming bond lengths in these TSs are longer than those of the forming bonds in the corresponding TSs of the cycloaddition between the less reactive cyclopentadiene and acrylonitrile at both HF/6-31G*[20] and B3LYP/6-31G*[21] theory levels, suggesting that *o*-QDM TSs, in accord with the Hammond postulate, are more reactant like than cyclopentadiene TSs.

Other characteristic geometrical features of these TSs, such as the sliding motion of the acrylonitrile moiety underneath

the diene moiety on going from both *endo* and *exo* TSs for the reactions of **1** and **2** to those for the reactions of **4** and **5**, are commented in detail for the related TSs of maleimide reactions.

Transition structures of *o*-QDMs with maleimide

Three couples of *endo*–*exo* isomeric TSs (Fig. 4) were located. They are all concerted and perfectly synchronous at HF and slightly asynchronous at B3LYP level of theory, although **28**–**31** TSs derive from symmetrical reactants. Asynchronicity in TSs arising from symmetric reactants is not a novelty in computational studies of Diels–Alder cycloadditions and it can be much more dramatic than that observed in our reactions.[22,23] Potential surface in the region of the TS is probably flat with the respect to the asymmetric stretching vibration that involve the two incipient bonds.

In order to describe some relevant aspects of TS geometries it is useful to focus our attention on the dihedral angles between the forming bond plane and both the diene (i.e. α=$C_{10}C_{9a}C_{5a}C_5$–$C_{10}C_5C_4C_{11}$) and dienophile heavy atom plane (β=$C_{10}C_5C_4C_{11}$–$C_1C_{11}C_4C_3$). In the TSs the carbon skeleton of both the QDM-diene and dienophile moieties are roughly confined to a plane.

As for *exo* TSs, on going from **28** to **30** and **32** one can observe a sliding motion of the maleimide moiety underneath the quinodimethane moiety accompanied by a clockwise (downward) rotation of the maleimide plane around the C_4–C_{11} bond. The sliding motion reduces both the α and β angles but in the case of the latter angle its effect is counteracted and overcome by the opposite, i.e. widening, effect of the downward maleimide rotation. Actually, there is a decrease by ≈13 and 9° in the α angle value in **30** and **32**, respectively, while the β angle widens by 3 and 7°. It seems that sliding is larger in **30** than in **32** while the rotation is the same in these TSs. Obviously, maleimide rotation also changes the dihedral angle between the diene and dienophile heavy atom planes; the angle between these planes is 167° in **28** and ≈183–184° in TSs **30** and **32** where they are almost parallel to each other.

The maleimide sliding motion as well as clockwise (now upward) rotation are observable also for *endo* TSs, i.e. on passing from **29** to **31** and **33**. Once again the former geometry change leads to a decrease in the α angle value by 13 and 6° in **31** and **33**, respectively. Also in *endo* TSs sliding motion and clockwise rotation have opposite effects on the β angle value but now the former gives rise to widening and the latter to narrowing. Moreover, they compensate each other almost exactly as shown by the remarkable substantial constancy of the β angle in *endo* TSs. The dihedral angle between the diene and dienophile heavy atom planes is ≈39° in **29**, 26° in **31** and 34° in **33** (Table 1).

It is quite evident that these dienophile motions take place in order to better accommodate the steric congestion of the aliphatic bridge and to lessen as far as possible the related non-bonded repulsive interactions.

The effect of steric repulsions should influence not only the approach geometry as discussed above but also they should give rise to reactant deformations (in the TSs) different for the *exo* as compared to the corresponding *endo* TSs.

Contribution of these deformations to the electronic activation barrier can be very easily obtained by calculating the energy necessary to deform the reactant geometries to those they assume in the TS, i.e. by single point calculation on the reactant deformed to their TS geometries. Thus, we computed, at B3LYP/6-31G* level, the contribution of the *reactant deformation* (E_{def}) to the electronic activation barriers ($\Delta E^{\neq}$) for the cycloaddition reactions of *o*-QDM **1**, **3** and **4** with maleimide. The deformation term always favors selectively the *endo* approach over the *exo* one and it contributes to the $\Delta\Delta E^{\neq}$ ($\Delta E^{\neq}_{exo}-\Delta E^{\neq}_{endo}$) by 0.66, 0.57 and 2.28 kcal mol^{-1} for the cycloaddition of maleimide with **1**, **3** and **4**, respectively. Such contribution represents 50, 61 and 93% of the *endo*–*exo* electronic energy difference. Thus we can confidently say that reactant deformation (caused by steric repulsions) in cycloaddition reactions involving *o*-QDMs and a reactive dienophile such as maleimide, is one of the main controlling factor of the *endo*–*exo* selectivity in the gas-phase.

And now a typical question concerning the DA cycloaddition reactions: is there evidence that the secondary orbital interactions play an important role in favoring the *endo* selectivity?

A quantitative answer requires a factorization of activation energy and we are still working in this field.[24] Nevertheless, there are few geometrical evidences which cast serious doubt on their role: (i) the carbon atoms C_{5a} and C_{9a} (Fig. 4) are always slightly *anti* pyramidalized with respect to the face attacked by the dienophile; (ii) the pyramidalization of such carbons is the same in *endo* and *exo* TSs;[†] (iii) the cycloaddition reaction of isoindene has the best *endo* TS geometry (smallest α and β angles of the series, i.e. α=103° and β=102° in the *endo* TS) for a maximization of secondary orbital interactions, but actually, it is the less *endo* selective (at the B3LYP level, see Table 2).

Although, no direct comparison to the DA cycloaddition of butadiene or cyclopentadiene with maleimide is possible, since no data are reported in the literature for the latter reactions, the forming bond lengths in TSs **28** and **29** are longer than those in TSs for the cycloaddition between isoprene and maleic anhydride[25] at the same level of theory. Thus, as emphasized above for TSs of *o*-QDM cycloadditions with acrylonitrile, also TSs for cycloadditions of *o*-QDMs with maleimide are more reactant-like than those for DA reactions of classical dienes.

Absolute reactivity

In order to assess the reliability of the computational approach in the reproduction of the experimental reactivity, we made a direct comparison of the absolute computed

[†] Pyramidalization of C_{5a} and C_{9a} carbon atoms, measured by $C_6C_{5a}C_{9a}C_5$ and $C_9C_{9a}C_{5a}C_{10}$ respectively, is: −173.2, 173.2° in **28**; −172.8, 172.8° in **29**; −176.7, 176.6° in **30**; −177.3, 177.1° in **31**; −171.2, 171.2° in **32**; −172.3, 172.1° in **33**.

Table 3. Solvent effect on activation Gibbs free energy ($\delta\Delta G^{\neq}_{MeCN}$) in kcal mol^{-1} [f]

Structures	$\delta\Delta G^{\neq}_{MeCN}$ (kcal mol^{-1})	$\Delta G^{\neq}_{MeCN}$ [a] (kcal mol^{-1})	$\Delta G^{\neq}_{MeCN,app}$ [b] (kcal mol^{-1})	$\Delta G^{\neq}_{exp}$ [d] (kcal mol^{-1})	$\Delta\Delta G^{\neq}_{MeCN}$ [c] (kcal mol^{-1})	$\Delta\Delta G^{\neq}_{exp}$ [c,e] (kcal mol^{-1})
exo TS **20**	−1.43	15.07	14.78	15.9	+0.28	–
endo TS **21**	−2.04	15.35				
exo TS **22**	−0.64	16.90	16.35	–	−0.25	−1.07
endo TS **23**	−1.61	16.65				
exo TS **24**	−1.45	16.97	16.46	–	−0.18	−0.72
endo TS **25**	−2.27	16.79				
exo TS **26**	−1.22	21.24	20.55	20.1	−0.47	−0.98
endo TS **27**	−2.49	20.77				
exo TS **28**	−1.14	13.58	12.50	11.4	−0.98	–
endo TS **29**	−1.20	12.60				
exo TS **30**	−1.47	15.23	12.23	–	−1.03	<−2.0
endo TS **31**	−1.91	12.33				
exo TS **32**	−0.96	20.91	17.49	14.7	−3.42	<−2.0
endo TS **33**	−2.12	17.49				

[a] $\Delta G^{\neq}_{MeCN}$ includes the $\delta\Delta G^{\neq}_{MeCN}$ correction ($\Delta G^{\neq}_{MeCN}=\Delta G^{\neq}+\delta\Delta G^{\neq}_{MeCN}$).
[b] Contribution of both *endo* and *exo* pathways: $\Delta G^{\neq}_{app}=\Delta G^{\neq}_{exo}+RT\ln[1+e^{(\Delta G^{\neq}_{exo}-\Delta G^{\neq}_{endo})/RT}]^{-1}$ if the *exo* TS is the most stable, or $\Delta G^{\neq}_{app}=\Delta G^{\neq}_{endo}+RT\ln[1+e^{(\Delta G^{\neq}_{endo}-\Delta G^{\neq}_{exo})/RT}]^{-1}$ if the *endo* TS is the most stable.
[c] A negative value means a more stable *endo* TS, vice versa a positive value means a more stable *exo* TS.
[d] Measured by flash photolysis in acetonitrile solution.
[e] Calculated from experimental *endo*–*exo* adduct ratios.
[f] Electrostatic solvent effect according to the Tomasi model (acetonitrile, ϵ=35.9) at the B3LYP/6-31G* level of theory. It is given as the difference between the solvent effect on the TSs and that on the reactants) and comparison between the theoretical absolute ($\Delta G^{\neq}_{MeCN}$), and relative activation Gibbs free energy ($\Delta\Delta G^{\neq}_{MeCN}=\Delta G^{\neq}_{MeCN,endo}-\Delta G^{\neq}_{MeCN,exo}$) with the experimental data ($\Delta G^{\neq}_{exp}$, $\Delta\Delta G^{\neq}_{exp}$, respectively.

Gibbs free activation energies ($\Delta G^{\neq}$) with the experimental values ($\Delta G^{\neq}_{exp}$). The latter were obtained from the measured second-order rate constant for DA reaction of **1** and **4**, generated in situ by flash photolysis (from 2-indanone and 1,2,3,4-tetrahydro-1,4-methanonaphthalen-9-one, respectively)[26] with acrylonitrile, maleimide and *N*-methylmaleimide. These data will be reported in detail elsewhere.[26] The kinetic experimental data for the cycloadditions involving **3** were not measured due to the lack of a suitable and efficient photochemical precursor. The second-order reaction rates of the cycloaddition involving the parent *o*-QDM **1** and 2,3-dihydronaphthalene **4** with acrylonitrile were measured in acetonitrile at 25°C (k=1.1(±0.2)×10^1, 1.3(±0.1)×10^{-2} M^{-1} s^{-1}). In a similar fashion we measured second-order reaction rates of the reaction of the parent *o*-QDM **1** and 2,3-dihydronaphthalene **4** with N–H maleimide (k_{N-H}=2.9(±0.1)×10^4, k_{N-H}=1.1(±0.1)×10^2 M^{-1} s^{-1}, for **1** and **4**, respectively). N–Me maleimide is roughly 10 times more reactive than the parent maleimide, showing second-order rate constants of 2.5(±0.1)×10^5 and 1.8(±0.1)×10^3 M^{-1} s^{-1}, for the cycloaddition reaction of **1** and **4**, respectively.

The corresponding activation free energies $\Delta G^{\neq}_{exp}$ (acetonitrile solution, Table 3) for the DA cycloaddition **1**+acrylonitrile, **1**+N–H maleimide, **4**+acrylonitrile and **4**+N–H maleimide are as follows: 15.9, 20.1, 11.4, 14.7 kcal mol^{-1}. Comparison between these experimental values in solution and the corresponding theoretical gas-phase $\Delta G^{\neq}$ values shows that the latter are always higher than the former by 0.6 –4.9 kcal mol^{-1} (Table 2). Notwithstanding such discrepancy, the reactivity order **1**>**4** is well reproduced computationally.

However, it should be emphasized that there is always an increase in the dipole moment on going from the reactants (e.g. μ=3.88 D for acrylonitrile, 1.49 D for maleimide, 0.12 D for **1**, 0.47 D for **3** and 0.57 D for **4**), to TSs (μ=4.18, 4.43, 4.67 and 4.71 D for **21**, **23**, **25**, and **27** TSs, respectively). Thus, if we want to compare theoretical and experimental absolute values we cannot neglect solvent effects, in particular electrostatic effects. Indeed, evaluation of electrostatic solvent effect through a PCM model (Tomasi) by single point calculation at the B3LYP/6-31G* level for polar acetonitrile (dielectric constant=35.9) demonstrated that both *endo* and *exo* TSs are stabilized with respect to the reactants by roughly 0.6–2.5 kcal mol^{-1} (see Table 3). The theoretical absolute apparent activation free energies, obtained taking into account both the *endo* and *exo* pathways ($k_{app}=k_{endo}+k_{exo}$), after correction with the solvent effect ($\Delta G^{\neq}_{MeCN,app}$) reproduce fairly well the experimental values ($\Delta G^{\neq}_{exp}$). The results are summarized in Table 3.

endo–*exo* Controlling factors

The computed gas-phase relative activation free energies $\Delta\Delta G^{\neq}$ ($\Delta G^{\neq}_{endo}-\Delta G^{\neq}_{exo}$, see Table 2) indicate a preference for the *exo* attack in acrylonitrile cycloadditions (by 0.6–0.9 kcal mol^{-1}), and for *endo* addition in maleimide (by 0.6–2.3 kcal mol^{-1}) reactions with *o*-QDMs **1**–**4**. The predicted distereoselectivity is substantially similar at both HF/6-31G* and B3LYP/6-31G* level of theory, even if without electronic correlation the preference for the *endo* TSs is slightly higher. The *exo* computational selectivity of the acrylonitrile gas-phase cycloadditions (see Table 1) is in contrast with the experimental results in acetonitrile solution (see $\Delta\Delta G^{\neq}_{exp}$ in Table 3, evaluated from the experimental *endo*–*exo* ratio) which show the *endo* attack to be preferred. On the other hand, the *endo* selectivity in maleimide cycloadditions with **1**–**4**, computed in gas-phase, is underestimated. However, it is well known that solvent effect can influence, usually by increasing, the *endo*–*exo* selectivity.[27] Thus, in order to computationally match the experimental results it is necessary to take into account the solvent effects.

The introduction of electrostatic solvent effect in calculations not only increases the predicted reactivity of the systems under study, as described in the preceding section, but it changes the relative *endo*–*exo* selectivity as well. In fact the *endo* TSs are stabilized in comparison with the *exo* TSs by 0.06–1.27 kcal mol^{-1} (Table 3). Selective *endo* stabilization by solvent effect in DA cycloadditions has already been described computationally, e.g. by Sustmann[28,29] and Ruiz–Lopez.[27,30] Anyway, even with the introduction of the solvent effect the computational *endo*–*exo* ratio is systematically underestimated by about 0.5 kcal mol^{-1}.

Such a discrepancy could be attributed to a systematic underestimation of the solvent effect at PCM level, because the dielectric continuum model is approximate and it is less accurate in polar solvent such as acetonitrile.[28]

It is clear from the results reported above that to describe in detail the reactivity and the *endo*–*exo* selectivity of *o*-QDM DA cycloadditions one must pay attention to solvent effect. In particular for cycloaddition involving acrylonitrile as dienophile the solvent becomes the controlling factor of the *endo*–*exo* selectivity, reverting the *exo* selectivity computed in the gas-phase.

Similar stabilization of the *endo* pathway by solvent effect is at work in the DA cycloadditions of *o*-QDMs **1**, **3** and **4** with maleimide as well, but the computational analysis of the DA cycloaddition reaction with such dienophile suggests that other *endo* orienting effects emerge clearly already in the gas-phase. We found, as described in the previous section, that steric effects, as a result of introduction of a methano or ethano bridge in *o*-QDM, not only give rise to significant changes in the geometry of approach between the two reaction partners but also can be held responsible of an energetically more expensive reactant deformation in *exo* as compared to the corresponding *endo* TSs. This deformation effect can account for a large part of the *endo*–*exo* energy difference.

Conclusion

The cycloaddition of *o*-QDMs to electron-poor olefins has been rationalized in the frame of a concerted mechanism. In fact, the involvement of a triplet diradical *o*-QDMs is unlikely because such a species is more than 22 kcal mol^{-1} less stable than the closed shell *o*-QDM **1**, and above all, it is even less stable than the TSs of the concerted cycloadditions with both acrylonitrile and maleimide.

The *endo* selectivity observed experimentally in *o*-QDMs cycloaddition reactions with acrylonitrile and more reactive dienophiles such as maleimide has been explained on the basis of a computational study at B3LYP/6-31G* level as a result of a selective *endo* electrostatic stabilization by a highly polar solvent such as acetonitrile, which is able even to revert the *exo* selectivity with acrylonitrile in the gas-phase. For a more reactive and rigid dienophile the preference for an *endo* approach (in the gas-phase) has been attributed mainly to deformation effects of both reagents in the TSs. Secondary orbital interactions if present do not appear to be particularly important in the control of the *endo*–*exo* selectivity, at least in Diels–Alder cycloadditions under study.

Noteworthy is the ability of the correlated calculation (DFT) to predict fairly well, with the inclusion of the solvation effects, the absolute and relative (*endo*–*exo*) reactivity of *o*-QDMs in DA cycloaddition reactions.

Experimental

Melting points are uncorrected. Elemental analyses were made on a Carlo Erba CNH analyzer, model 1106. Infrared spectra were recorded as KBr discs, nujol or films on a Perkin–Elmer FT1000 spectrophotometer. ^{1}H and ^{13}C NMR spectra were recorded in $CDCl_3$ solutions (unless otherwise stated) on a Bruker AE 300 spectrometer with Me_4Si as internal standard. Protons were correlated by decoupling and COSY experiments, while protons were correlated to carbons by ^{1}H–^{13}C heterocorrelated spectra. GC analyses were performed with a DANI 6500, PTV injector, CP-Sil 19CB (25 m) capillary column using H_2 as a carrier. Preparative column chromatography was performed on Merck Silica gel 60 (79–230 mesh) using cyclohexane–ethyl acetate mixtures (from 95:5 to 60:40) unless otherwise stated.

[*o*-((Trimethylsilyl)methyl)benzyl]trimethylammonium iodide (**5**), [α-[*o*-[α-(trimethylsilyl)ethyl]phenyl]ethyl]trimethylammonium iodide (**6**), [1-(trimethylsilyl)-1,2,3,4-tetrahydronaphth-4-yl] trimethylammonium iodide (**8**) were prepared according to published literature.[10] Adducts **9**, **18endo** and **18exo** have been already characterized.[10]

[1-(Trimethylsilyl)-3-dimethylamino]indan. To a solution of *N*,*N*-dimethyl-1-indanylamine[31] (4.5 g, 27.90 mmol) in diethylether (90 ml), 1.6 M *n*-BuLi in hexane (45 ml, 72.0 mmol) was added at room temperature. The solution was stirred for 22 h at room temperature. A mixture of TMSCl (9 ml, 70.91 mmol) and triethylamine (1 ml) was added to the resulting reddish solution all at once at 0°C. After being stirred at room temperature for 2 h, the mixture was quenched with cold aqueous sodium carbonate and extracted with ether. The ether extract was washed with brine and evaporated to give a mixture of [1-(trimethylsilyl)-3-dimethylamino]indan, [1-(dimethylamino)-7-trimethylsilyl]indan and [1,1-(bis(trimethylsilyl))-3-dimethylamino]indan. The mixture was dissolved in 10 M sulfuric acid (50 ml) and acetic acid (70 ml) and heated at 50°C for 8 h.

The reaction mixture was made alkaline by addition of solid sodium carbonate and extracted with ether. The ether extract was washed with brine and dried over $MgSO_4$. Evaporation of the solvent followed by vacuum distillation afforded 3.8 g (58.3% yield) of the desired product as a colorless oil [bp 103°C (0.3 mmHg)]: IR (nujol) 1249, 899, 838 cm^{-1}. ^{1}H NMR ($CDCl_3$) δ 0.11 (s, 9H, TMS), 1.93 (ddd, 1H, J=13.0, 8.0, 3.9 Hz), 2.25 (s, 6H), 2.31 (ddd, 1H, J=13.0, 10.0, 8.0 Hz), 2.50 (dd, 1H, J=10.0, 3.9 Hz), 4.32 (t, 1H, J=8.0 Hz), 7.05–7.18 (m, 4 H). Anal. Calcd for $C_{14}H_{23}NSi$: C, 72.04; H, 9.93; N, 6.00; Si, 12.03. Found: C, 71.95; H, 9.92; N, 6.05.

[1-(Trimethylsilyl)-indan-4-yl] trimethylammonium iodide (7). A solution of [1-(trimethylsilyl)-3-dimethylamino]-indan (820 mg, 3.52 mol) and methyl iodide (1.6 ml, 25.6 mmol) in acetonitrile solution was refluxed for 2 h. A large amount of ether was added to precipitate [1-(trimethylsilyl)-indan-4-yl]trimethylammonium iodide which was washed with ethyl acetate to obtain 1.1 g (83% yield) of **7** as a white solid: mp 181±1°C (from ethyl acetate); IR (nujol) 1467, 1250, 840 cm^{-1}. ^1H NMR ($CDCl_3$) δ 0.80, (s, 9H), 2.72–2.89 (m, 2H), 3.34 (s, 9H), 3.55 (m, 1H), 5.24 (m, 1H, *J*=8.1 Hz), 7.21–7.78 (m, 4H). Anal. Calcd for $C_{15}H_{26}NISi$: C, 48.00; H, 6.98; N, 3.73; I, 33.81; Si, 7.48. Found: C, 48.04; H, 7.01; N, 3.74.

Cycloaddition of *o*-quinodimethanes with dienophiles (general procedures)

Method A: This method is exemplified by synthesis of 3a,4,9,9a-tetrahydro-3H-naphtho[2,3-C]furan-1-one.

(3ar, 9ac)-3a,4,9,9a-Tetrahydro-3*H*-naphtho[2,3-C]furan-1-one (10). To a deoxygenated solution of **5** (100 mg, 0.27 mmol) and 2-(5H)-furanone (260 mg, 3.10 mmol) solid KF (100 mg, 1.73 mmol) was added. The resulting suspension was boiled for 5 h. The reaction mixture was cooled, diluted with ether and the insoluble material was filtered off.

The filtrate was concentrated, and purified by column chromatography on silica gel (eluent=cyclohexane–ethyl acetate=6:4) to give **10** (28 mg, 54% yield) as a white crystalline solid: mp 135±1°C; IR (nujol) 1756, 1151, 1019, 755 cm^{-1}; ^1H NMR ($CDCl_3$) δ 2.59 (dd, 1H, *J*=14.4, 5.8 Hz), 2.86 (dd, 1H, *J*=14.4, 5.8 Hz), 2.93–3.14 (m, 4H, *J*=3.0, 15.0 Hz), 3.86 (dd, 1H, *J*=2.9, 8.6 Hz), 4.47 (t, 1H, *J*=8.6 Hz), 7.09–7.21 (m, 4H). Anal. Calcd for $C_{12}H_{12}O_2$: C, 76.57, H, 6.43; O, 17.00. Found: C, 76.48, H, 6.41.

Method B: This method is exemplified by the synthesis of 2-methyl-3a,4,9,9a-tetrahydro-benzo[f]isoindole-1,3-dione.

2-Methyl-(3ar,9ac)-3a,4,9,9a-tetrahydro-benzo[f]isoindole-1,3-dione (11). To a degassed solution of **5** (100 mg, 0.27 mmol) and *N*-methylmaleimide (40 mg, 0.36 mmol) in 1 ml of acetonitrile was added a degassed solution of TBAF (91 mg, 0.29 mmol) in 5 ml of acetonitrile over 40 min at room temperature. The resulting pink solution was stirred for 1 h, the reaction mixture was diluted with ether and the insoluble materials were filtered off.

The filtrate was concentrated, and column chromatography on silica gel of the residue gave 41 mg (69%) (eluent=cyclohexane–ethylacetate=7:3) of **11** as a white crystalline solid: mp 138±1°C; IR (nujol) 1693, 1281, 769 cm^{-1}; ^1H NMR ($CDCl_3$) δ 2.77 (s, 3H), 2.92 (dd, 2H, *J*=3.0, 15 Hz), 3.12 (dd, 2H, *J*=3.0, 15.0 Hz), 3.28 (t, 2 H, *J*=3.0 Hz), 7.11–7.20 (m, 4H). Anal. Calcd for $C_{13}H_{13}NO_2$: C, 72.54, H, 6.09, N, 6.51; O, 14.87. Found: C, 72.59; H, 6.10, N, 6.55.

1,4-Dimethyl-2-cyano-1,2,3,4-tetrahydronaphthalene (12endo and 12exo). To a degassed solution of **6** (230 mg, 0.59 mmol) in 4 ml of acetonitrile–acrylonitrile=1:1 mixture, a degased solution of TBAF (240 mg, 0.76 mmol) in 10 ml of acetonitrile was added over 1 h at room temperature. The resulting solution was stirred for an additional hour. The reaction mixture was diluted with ether and insoluble material was filtered off.

The filtrate was concentrated, and column chromatographed on silica gel to give 50 mg (49%, yield) (eluent=cyclohexane–ethyl acetate=8:2) of a mixture of **12endo** and **12exo** (84:16) as an oil. *endo–exo* Ratio was evaluated by ^1H NMR on the reaction mixture. Adducts **12endo** and **12exo** were characterized in mixture.

12endo. ^1H NMR ($CDCl_3$) δ 1.40 (d, 3H, *J*=6.8 Hz), 1.47 (d, 3H, *J*=7.1 Hz), 1.84 (ddd, 1H, *J*=13.4, 12.2, 11.1 Hz), 2.22 (dddd, 1H, *J*=13.4, 6.3, 3.4, 1.0 Hz), 2.87–2.98 (m, 1H) 3.02–3.10 (ddd, 1H, *J*=12.2, 4.9, 3.4 Hz), 3.11–7.22 (m, 1H), 7.11–7.20 (m, 4H).

12exo. ^1H NMR ($CDCl_3$) δ 1.35 (d, 3H, *J*=7.1 Hz), 1.51 (d, 3H, *J*=7.1 Hz), 1.92–1.99 (ddd, 1H, *J*=13.5, 6.2, 3.8 Hz), 2.12 –2.18 (ddd, 1H, *J*=13.5, 9.0, 5.7 Hz), 2.87–2.98 (m, 1H, signal overlapped to **12endo** isomer), 2.78 (ddd, 1H, *J*=9.0, 8.0, 3.8 Hz), 3.11–7.22 (m, 1H, signal overlapped to **12endo** isomer), 7.15–7.24 (m, 4H).

12endo+12exo. IR (nujol) 2236, 750 cm^{-1}; Anal. Calcd for $C_{13}H_{15}N$: C, 84.28, H, 8.16, N, 7.56. Found: C, 84.35; H, 8.19, N, 7.52.

2,4,9-Trimethyl-(3ar,4c,9c,9ac)-3a,4,9,9a-tetrahydro-benzo-[f]isoindole-1,3-dione (13endo). The reaction gave only the *endo* adduct as a white crystalline solid (86% yield) purified by column chromatography on silica gel (eluent=cyclohexane–ethyl acetate=7:3). Mp 154±1°C; IR (nujol) 1698, 1283, 755 cm^{-1}.; ^1H NMR ($CDCl_3$) δ 1.67 (d, 6H, *J*=7 Hz), 2.47 (s, 3H), 2.91–3.02 (m, 2H), 3.10–3.15 (m, 2H), 7.11–7.20 (m, 4H); ^{13}C NMR ($CDCl_3$) 14.1, 24.1, 32.6, 45.0, 123.6, 126.8, 138.3, 177.1. Anal. Calcd for $C_{15}H_{17}NO_2$: C, 74.05, H, 7.04, N, 5.76; O, 13.15. Found: C, 74.05; H, 7.04, N, 5.76.

2-Cyano-4,5-benzobicyclo[2.2.1]eptane (16endo and 16exo). According to the Procedure B, **16endo** and **16exo** were prepared in low yield (12 mg, 14%) starting from **7** (200 mg, 0.53 mmol). *endo–exo* Ratio (77:23) was evaluated by ^1H NMR on the reaction mixture. Adducts **16endo** and **16exo** were isolated by column chromatography on silica gel (eluent=cyclohexane–ethylacetate=9:1), both as colorless oil.

16endo. IR (nujol) 2246, 742 cm^{-1}. ^1H NMR ($CDCl_3$) δ 1.46 (ddd, 1H, *J*=12.0, 4.1, 2.7 Hz), 1.61 (dt, 1H, *J*=9.5, 1.5 Hz), 1.93 (ddd, 1H, *J*=9.5, 4.5, 2.7 Hz), 2.39 (ddd, 1H, *J*=12.0, 10.5, 3.9 Hz), 3.12 (ddd, 1H, *J*=10.5, 4.1, 3.9 Hz), 3.48 (m, 1H) 3.64 (m, 1H), 7.13–7.38 (m, 4H). Anal. Calcd for $C_{12}H_{11}N$: C, 85.19, H, 6.52, N, 8.28. Found: C, 85.30; H, 6.50, N, 8.24.

16exo: IR (nujol) 2241, 735 cm^{-1}. ^1H NMR ($CDCl_3$) δ 1.43 (ddd, 1H, *J*=12.0, 10.5, 2.5 Hz), 1.59 (dt, 1H, *J*=9.5,

1.5 Hz), 1.93 (ddd, 1H, *J*=9.5, 4.5, 2.5 Hz), 2.73 (dd, 1H, *J*=12.0, 3.9 Hz), 2.94 (m, 1H), 3.40 (m, 1H) 3.64 (m, 1H), 7.10–7.28 (m, 4H). Anal. Calcd for $C_{12}H_{11}N$: C, 85.17, H, 6.55, N, 8.28. Found: C, 85.28; H, 6.47, N, 8.20.

2-Methyl-(3ac,9ac)-3a,4,9,9a-tetrahydro-4r,9c-methanobenzo[f]isoindole-1,3-dione (15endo). Starting from **7** (150 mg, 0.39 mmol) and N–Me maleimide (66.5 mg, 0.59 mmol) according to Method B, **15endo** was obtained as a single adduct in white crystals (47 mg, 69% yield) from cyclohexane–ethylacetate=7:3; mp 155±1°C; IR (nujol) 1698, 1283, 755 cm^{-1}.; ^1H NMR ($CDCl_3$) δ 1.91 (dt, 1H *J*=9.5, 1.5 Hz), 2.10 (dt, 1H, *J*=9.5, 1.5 Hz), 2.28 (s, 3H), 3.47 (m, 2H), 3.82 (m, 2H), 7.08–7.19 (m, 4H); ^{13}C NMR ($CDCl_3$) 23.5, 46.1, 47.4, 122.6, 126.9, 141.8, 176.8. Anal. Calcd for $C_{14}H_{13}NO_2$: C, 73.99, H, 5.77, N, 6.16; O, 14.08. Found: C, 74.07; H, 5.71, N, 6.18.

2-Methyl-(3ac,9ac)-3a,4,9,9a-tetrahydro-4r,9c-ethanobenzo[f]isoindole-1,3-dione (17endo). Starting from **8** (125 mg, 0.32 mmol) and N–Me maleimide (71 mg, 0.64 mmol) according to Method B, **17endo** was obtained as a single adduct in white crystals (52 mg, 67% yield) from cyclohexane–ethylacetate=7:3; mp 195±1°C; IR (nujol) 1695, 1283 cm^{-1}; ^1H NMR (C_6D_6) δ 1.08 (m, 2H), 1.25 (m, 2H), 2.25 (s, 3H), 2.38 (m, 2H), 3.30 (m, 2H), 6.96–7.01 (m, 4H); ^{13}C NMR (C_6D_6) 24.1, 24.7, 45.0, 125.5, 127.6, 139.2, 177.6. Anal. Calcd for $C_{15}H_{15}NO_2$: C, 74.67, H, 6.27, N, 5.81; O, 13.26. Found: C, 74.59; H, 6.23, N, 5.84.

4,9-Dimethyl-(3ar,9ac)-3a,4,9,9a-tetrahydro-3H-naphtho-[2,3-C]furan-1-one (14endo and 14exo). Starting from **6** (100 mg, 0.26 mmol), 2-(5H)-furanone (231 mg, 2.75 mmol), KF (100 mg, 1.72 mmol) in 3 ml of acetonitrile according to the Procedure A, two adducts (18 mg, 33%) were recovered as white crystalline solids, **14endo** (94%) and **14exo** (6%) purified by column chromatography on silica gel (eluent=cyclohexane–ethyl acetate=6:4).

14endo. Mp 146±1°C; IR (nujol) 1757, 1170, 759 cm^{-1}; ^1H NMR (C_6D_6) δ 1.39 (d, 3H, *J*=7.1 Hz), 1.71 (d, 3H, *J*=6.8 Hz), 2.95–3.23 (m, 4H), 3.48 (dd, 1H, *J*=9.3, 6.4 Hz), 4.15 (t, 1H, *J*=9.3 Hz), 7.19–7.30 (m, 4H). ^1H NMR ($CDCl_3$) δ 0.82 (d, 3H, *J*=7.1 Hz), 1.68 (d, 3H, *J*=6.8 Hz), 2.15–2.25 (m, 2H), 2.32–2.43 (m, 2H), 3.05 (dd, 1H, *J*=9.3, 6.4 Hz), 3.45 (t, 1H, *J*=9.3 Hz), 7.05–7.15 (m, 4H). Anal. Calcd for $C_{14}H_{16}O_2$: C, 77.75, H, 7.46, O, 14.80. Found: C, 77.68; H, 7.49.

14exo. Mp 158±1°C; IR (nujol) 1752, 1177, 746 cm^{-1}; ^1H NMR (C_6D_6) δ 1.38 (d, 3H, *J*=7.1 Hz), 1.70 (d, 3H, *J*=6.8 Hz), 2.88–3.15 (m, 3H), 3.72 (dd, 1H, *J*=9.3, 6.6 Hz), 4.42 (t, 1H, *J*=9.3 Hz), 7.08–7.25 (m, 4H). ^1H NMR ($CDCl_3$) δ 0.80 (d, 3H, *J*=7.1 Hz), 1.55 (d, 3H, *J*=6.8 Hz), 2.15–2.30 (m, 2H), 2.40–2.48 (m, 2H), 3.15 (dd, 1H, *J*=9.3, 6.4 Hz), 3.62 (t, 1H, *J*=9.3 Hz), 7.05–7.15 (m, 4H). Anal. Calcd for $C_{14}H_{16}O_2$: C, 77.75, H, 7.46, O, 14.80. Found: C, 77.70; H, 7.40.

(3ac,9ac)-3a,4,9,9a-tetrahydro-4r,9c-ethano-3*H*-naphtho-[2,3-C]furan-1-one (19endo). Starting from **8** (150 mg, 0.38 mmol), 2-(5H)-furanone (323 mg, 3.84 mmol), KF (150 mg, 2.59 mmol) in 3 ml of acetonitrile according to the Procedure A, a single *endo* adduct was recovered as a white crystalline solid (14 mg, 17%), which was purified by column chromatography on silica gel (eluent=cyclohexane–ethyl acetate=7:3). Mp 130±2°C; IR (nujol) 1752 1175, 765 cm^{-1}; ^1H NMR ($CDCl_3$) δ 1.49–1.58 (m, 2H), 1.72–1.91 (m, 2H), 2.94–3.01 (m, 2H), 3.01–3.06 (m, 1H), 3.48–3.51 (m, 1H), 3.58–3.63 (m, 1H), 4.28–4.33 (m, 1H), 7.18–7.28 (m, 4H). Anal. Calcd for $C_{14}H_{14}O_2$: C, 78.48, H, 6.59, O, 14.93. Found: C, 78.33; H, 6.63.

Acknowledgements

Financial support from MURST and CNR is gratefully acknowledged.

References

1. Charlton, J. L.; Alauddin, M. M. *Tetrahedron* **1987**, *43*, 2873.
2. Mann, J.; Piper, S. E.; Yeung, L. K. P. *J. Chem. Soc., Perkin Trans. 1* **1984**, 2081.
3. Kametani, T.; Fukumoto, K. *Med. Res. Rev.* **1981**, *1*, 23.
4. Quinkert, G.; Stark, H. *Angew. Chem., Int. Ed. Engl.* **1983**, *22*, 637.
5. Kametani, T.; Nemoto, H. *Tetrahedron* **1981**, *37*, 3.
6. Nemoto, H.; Fukumoto, K. *Tetrahedron* **1998**, *54*, 5425.
7. Segura, J. L.; Martín, N. *Chem. Rev.* **1999**, *99*, 3199 and references therein.
8. Kametani, T.; Honda, T.; Ebisawa, Y.; Ichikawa, H. *Tetrahedron* **1985**, *41*, 3643.
9. Durst, T.; Kozma, E. C.; Charlton, J. C. *J. Org. Chem.* **1985**, *50*, 4829.
10. Ito, Y.; Nakatsuka, M.; Saegusa, T. *J. Am. Chem. Soc.* **1980**, *102*, 863.
11. Ginsberg, D. *Tetrahedron* **1983**, *39*, 2995.
12. Charlton, J. L.; Alauddin, M. M.; Penner, G. H. *Can. J. Chem.* **1986**, *64*, 793.
13. Wagner, P. J.; Sobczak, M.; Park, B.-S. *J. Am. Chem. Soc.* **1998**, *120*, 2488.
14. Arnold, B. J.; Mellows, S. M.; Sammes, P. G.; Wallace, T. W. *J. Chem. Soc., Perkin Trans. 1* **1974**, 401.
15. Bovio, B. Personal communication.
16. Becke, A. D. *J. Chem. Phys.* **1993**, *98*, 1372.
17. Lee, C.; Yang, W.; Parr, R. G. *Phys. Rev. B* **1988**, *37*, 785.
18. Frisch, M. J.; Trucks, G. W.; Schlegel, H. B.; Gill, P. M. W.; Johnson, B. G.; Robb, M. A.; Cheeseman, J. R.; Keith, T.; Petersson, G. A.; Montgomery, J. A.; Raghavachari, K.; Al-Laham, M. A.; Zakrzewski, V. G.; Ortiz, J. V.; Foresman, J. B.; Cioslowski, J.; Stefanov, B. B.; Nanayakkara, A.; Challacombe, M.; Peng, C. Y.; Ayala, P. Y.; Chen, W.; Wong, M. W.; Andres, J. L.; Replogle, E. S.; Gomperts, R.; Martin, R. L.; Fox, D. J.; Binkley, J. S.; Defrees, D. J.; Baker, J.; Stewart, J. P.; Head-Gordon, M.; Gonzalez, C.; Pople, J. A. GAUSSIAN 94, Revision E.3; Gaussian, Inc.: Pittsburgh, PA, 1995.
19. Tomasi, J.; Persico, M. *Chem. Rev.* **1997**, *94*, 2027.
20. Jorgensen, W. L.; Lim, D.; Blake, J. F. *J. Am. Chem. Soc.* **1993**, *115*, 2936.
21. Branchadell, L. *Int. J. Quant. Chem.* **1997**, *61*, 381.
22. Chen, J. S.; Houk, K. N.; Foote, C. S. *J. Am. Chem. Soc.* **1998**, *120*, 12302.
23. McCarrick, M. A.; Wu, Y.; Houk, K. N. *J. Org. Chem.* **1993**, *58*, 3330.

24. Di Valentin, C.; Rastelli, A.; Gandolfi, R. In preparation.
25. Beno, B. R.; Houk, K. N.; Singleton, D. A. *J. Am. Chem. Soc.* **1996**, *118*, 9984.
26. Freccero, M.; Gandolfi, R.; Sarzi-Amadè, M. In preparation.
27. Cativiela, C.; Garcìa, J. I.; Mayoral, J. A.; Salvatella, L. *Chem. Soc. Rev.* **1996**, 209.
28. Karcher, T.; Sicking, W.; Sauer, J.; Sustamann, R. *Tetrahedron Lett.* **1992**, *33*, 8027.
29. Sustamann, R.; Sicking, W. *Tetrahedron* **1992**, *48*, 10293.
30. Ruiz-Lòpez, M. F.; Assfeld, X.; Garcìa, J. I.; Mayoral, J. A.; Salvatella, L. *J. Am. Chem. Soc.* **1993**, *115*, 8780.
31. Brewster, J. H.; Buta, J. G. *J. Am. Chem. Soc.* **1966**, *88*, 2233.